ARTICLE

Supperlattice-Like Structure: Ordered Mass Transfer Endowing High Quality Output of Fuel Cell

Jian Wang [a,#], Wen-Hui Xuan [a,#], Qian He [a], Jing-Xia Jiang [a], Yuan-Yuan Zhou [a], Yao Nie [b], Qiang Liao [c], Min-Hua Shao [d], Wei Ding [a,*], Zi-Dong Wei [a,*]

[a] Chongqing Key Laboratory of Chemical Process for Clean Energy and Resource Utilization, School of Chemistry and Chemical Engineering, Chongqing University, Chongqing 401331, China
[b] Chongqing Key Laboratory of Green Synthesis and Applications, College of Chemistry, Chongqing Normal University, Chongqing 401331, China
[c] Institute of Engineering Thermophysics, School of Energy and Power Engineering Chongqing University, Chongqing 400044, China
[d] Department of Chemical and Biomolecular Engineering, The Hong Kong University of Science and Technology, Clear Water Bay, Kowloon 999077, Hong Kong

Abstract

The current or voltage fluctuation in fuel cell operation is harmful to the fuel cell system and power application equipment. Here, we report a technique to eliminate such a fluctuation by the aid of new type of catalysts, superlattice-like mesoporous PtCo catalysts. The current fluctuation in fuel cells catalyzed by two invented catalysts are fixed at as low as 25 $mA \cdot cm^{-2}$ with a power of 0.75 $W \cdot cm^{-2}$ or 120 $mA \cdot cm^{-2}$ with a power of 1.01 $W \cdot cm^{-2}$, and no noticeable current decay was detected over 100 h. By contrast, a cell catalyzed by conventional Pt/C catalysts with the same Pt loading delivered a current fluctuation as large as 180 $mA \cdot cm^{-2}$ even at low power output of 0.30 $W \cdot cm^{-2}$, which also showed 32% current decay rate in 50 h. The superlattices-like mesoporous structure not only enhances the mass transfer and depresses the water flooding but also effectively increases the Pt utilization within its 3D carbon frameworks. Its power output was as high as 11.69 $W \cdot mg_{Pt}^{-1}$ (MEA), which is 46.1% higher than the 2025 target of DOE, USA, 8.0 $W \cdot mg_{Pt}^{-1}$ (MEA).

Keywords: Quality output; Superlattices-like; PtCo alloy; Mass transport; ORR

1. Introduction

Proton exchange membrane fuel cell (PEMFC) systems have wide application prospects, including electric power stations, automotive transportations, and aircraft applications [1—3]. The fuel cell, where the electrochemical reaction occurs, is a strong coupling, complex nonlinear, multi-input and multi-output energy transform device. The outputting current and voltage of fuel cells are liable to fluctuate with the O_2 supply content and the water draining situation, which not only increases the cost of power generation system but also decreases the lifetime of electric device and the power quality [4,5]. Thus, it is necessary to rectificate current/voltage fluctuation before load access [6,7]. Many assistant electric devices, including DC—DC converters, ultra-capacitors, energy management systems and so on, are needed to decrease the fluctuation of current/voltage output to realize the demanded electricity quality during the practical applications [8—10]. In addition, the balance of mass transfer and activity performance in catalyst layer also plays an important role in the fluctuation of current/voltage output, especially, the phenomenon of catalyst layer flooding often occurs as a result of liquid production and vapor condensation, and pore filling or localized film formation, resulting in a significant decrease in the diffusion of reactant gases to the catalyst sites. Compared to extensive efforts to understand the flooding mechanisms, and improve the performance of anti-flooding in catalyst layer, the common approaches to reduce

Received 31 May 2022; revised 24 July 2022; accepted 5 October 2022; Available online 8 October 2022

* Corresponding author, Wei Ding, Tel: (86-23)65678931, E-mail address: dingwei128@cqu.edu.cn.
* Corresponding author, Zi-Dong Wei, Tel: (86-23)65678931, E-mail address: zdwei@cqu.edu.cn.
#These authors contributed equally to this work.

https://doi.org/10.13208/j.electrochem.2215003

the catalyst flooding are (1) to introduce hydrophobic additive to the catalyst layer and (2) to design the structure of catalyst layer. However, little attention has been received to balance the fluctuation of current/voltage output and the design of anti-flooding catalyst layer [11−15]. Ordering catalytic layers in the membrane electrode assembly (MEA) to improve Pt utilization and enhance mass transport has been regarded as an effective strategy to improve the performance of anti-flooding [16−18]. However, the ordered ultrathin catalyst layer always suffers from water flooding due to lack of enough space for water transportation [19,20], leading to vibratory power output as the discontinuous dewatering. A superlattice (SL), where two or more different materials are grown to a specific thickness, showed automatically arranged and interparticle spaced structure [21−25]. The former could endow an automatic connection among active sites, and the later would allow full access to active constituents with enhanced mass transport properties. Therefore, the rational design, and introduce the SL structure into the catalyst itself and catalyst layer with enough space are supposed to realize high performance of fuel cell.

Herein, we reported a template-assisted epitaxial assembly strategy that produced a superlattice-like nitrogen doped carbon framework with the modulated space for water transport. As shown in Fig. 1a, the home-made ultrathin Co-Al layered double hydroxide nanosheets (CoAl-LDH) were used as templates. After dehydration, the Co atoms exposed on the surface were served as nucleation seeds of zeolite imidazole framework-67 (ZIF-67). Then, the PVP-capped Pt nanoparticles (PVP-Pt NPs) were dispersed into the superlattice-like structure during the in-situ growth of ZIF-67 crystals. After controlled pyrolysis in H_2-N_2 atmosphere at 800 °C, the LDH-ZIF precursors were transformed into ordered mesoporous carbon polyhedron crystals with superlattice-like structure and Pt_3Co (Figure S1). The resulted catalysts were denoted as Pt_3Co@C-SLS-x, where SLS means superlattice-like structure, and x denotes the mole ratio of Co/Al. It was found that modulating the ratio of Co to Al atoms on the surface of CoAl LDH is key to control the surface density of ZIF-67 crystals. The lower ratio of Co/Al atoms led to the lower surface density and the larger particle size of ZIF-67 crystals, meaning that a larger space was produced between ZIF-67 crystals. The experimental results showed that the surface density of ZIF crystals largely determined the anti-flooding ability and quality of power output. A fuel cell catalyzed by the invented catalysts could output a power of 0.75 $W \cdot cm^{-2}$ with a current fluctuation as small as 25 $mA \cdot cm^{-2}$ over 100 h. Besides, the highest Pt utilization (11.69 $W \cdot mg_{Pt}{}^{-1}$ (MEA)) had been achieved so far with the invented Pt_3Co@C-SLS-x catalysts.

2. Results and discussion

The procedure for the synthesis of superlattice-like catalyst is illustrated in Fig. 1a, and monitored by using X-Ray Diffraction (XRD). All XRD peak intensities of LDH dramatically decreased after the growth of ZIF crystals (Figure S1a), indicating the collapse of the layered LDH structure. This was due to the attachment of ZIF crystals on each LDH layer, where the surficial hydroxyl groups were removed and Co atoms were exposed in the surface modification. The layered structure collapsed more seriously as the increased Co content of LDH, evidenced by the decreased XRD peaks intensity of LDH (Figure S1b and c, Figure S2). These results indicated that the interaction between ZIF-67 crystals and LDH layers could be further enhanced with the increased anchor sites for ZIF crystal seed formation. The scanning electron microscopic (SEM) and high-resolution transmission electron microscopic (HR-TEM) images confirmed that the ZIF crystals were uniformly grown on the surface of LDH to form the ZIF and LDH cross distributed superlattice-like structure (Fig. 1b−h). After controlled pyrolysis, ZIF-67 crystals were transformed into porous carbon framework and the PVP-Pt NPs were alloyed with Co due to the thermal diffusion of Co atoms from LDH or ZIF-67 to Pt NPs (Fig. 1 and S1a). The particle size of PtCo alloy was kept at ~3 nm according to the XRD results and TEM images even after high temperature pyrolysis at 800 °C (Fig. 1e). The HR-TEM observation showed that the LDH templates were totally removed, and the produced carbon-based catalyst perfectly remained the original superlattice-like structure (Fig. 1f). The elemental mappings displayed that the Co and Pt were uniformly distributed within the superlattices-like structure. Such superlattice-like structure would endow large and well-connected space for mass transfer which might promote the Pt utilization and antiflooding capability. Fig. 1g and h showed that the hollow PtCo NPs were anchored by the graphitic carbon shell, and a few Co single atoms dispersed on the surface. The STEM-electron energy loss spectroscopic (STEM-EELS) line scans confirmed the hollow structure with the Pt-rich surface for PtCo NPs (Fig. 1i).

The Co content had a tiny impact on the layered structure of Co-Al LDH, however, it dramatically

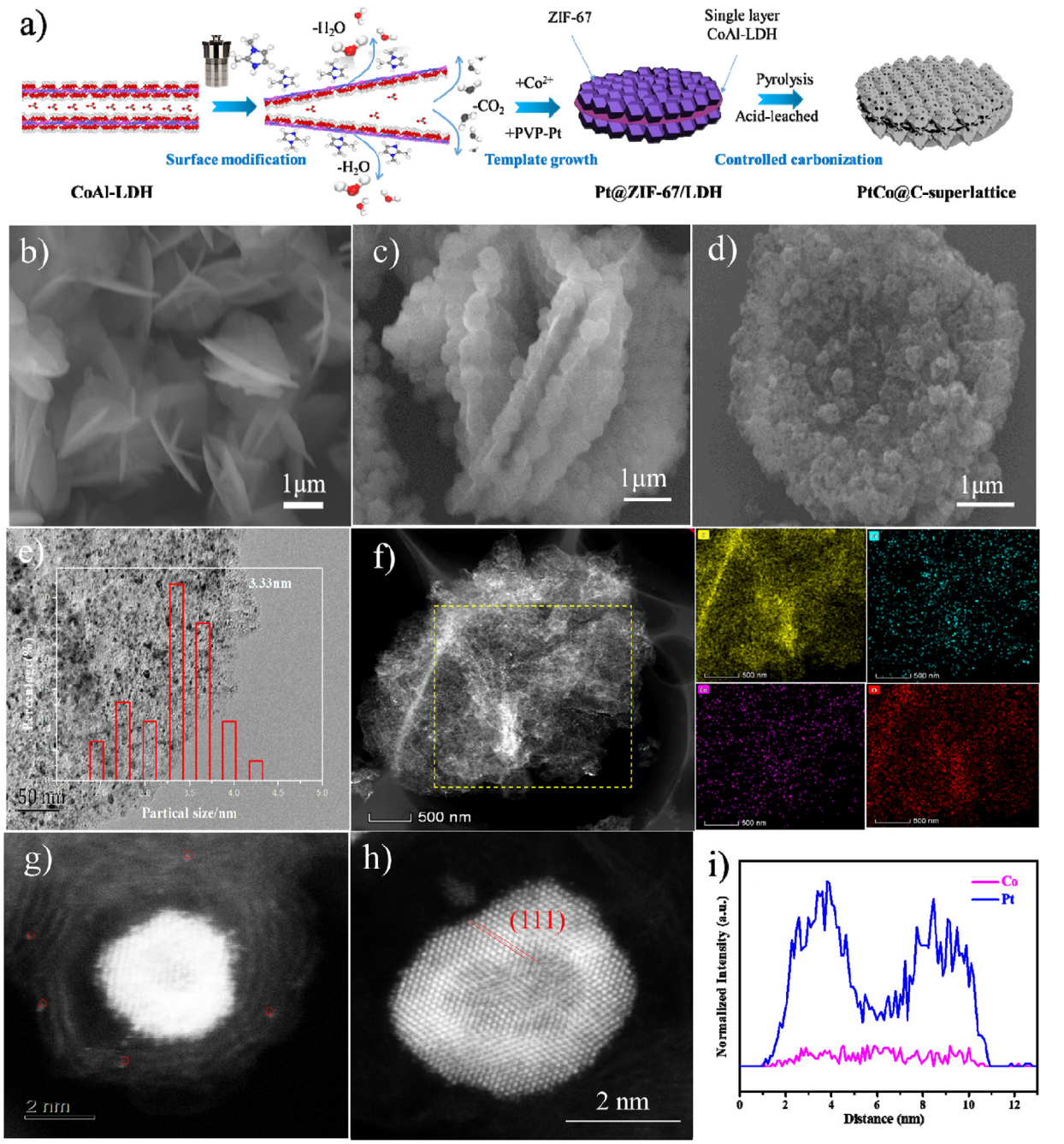

Fig. 1. (a) Schematic illustration of the synthetic procedure of Pt_3Co@SLs-MCPTx catalyst, (b) SEM image of CoAl-LDH-2. (c) SEM image of Pt@SLs-ZIF-67-LDH-2. (d) SEM image of the Pt_3Co@SLs-MCPT2 after the controlled pyrolysis process of Pt@SLs-ZIF-67-LDH-2. (e) TEM image of the Pt_3Co@SLs-MCPT2. (f) Atomic resolution HAADF-STEM image of Pt_3Co@SLs-MCPT2 and elemental mappings, (g) Atomic resolution HAADF-STEM image of PtCo nanoparticle. (h) Dark-field STEM image of Pt_3Co@SLs-MCPT2, (i) STEM-EELS line scan of Pt_3Co nanoparticle.

changed the ZIF growth as well as the meso-scale property of the final catalyst (Fig. 1b and S3). As shown in Fig. 2, the density of ZIF-67 on the LDH surface increased as the Co content increased, and the particle size of ZIF-67 crystals decreased accordingly. Eventually, the density of derived carbon framework increased with the increase of Co content. The mesoporous structure was even transformed into a packing flat structure when the Co/Al ratio increased to 6/1 (Fig. 2h). The Brunauer-Emmet-Teller (BET) specific surface area of catalysts, obtained by nitrogen isotherm adsorption, increased from 566 to 704 $m^2 \cdot g^{-1}$ when the Co/Al ratio increased from 1 to 2. Further increased the Co/Al ratio, however, led to dramatically decrease of BET surface area

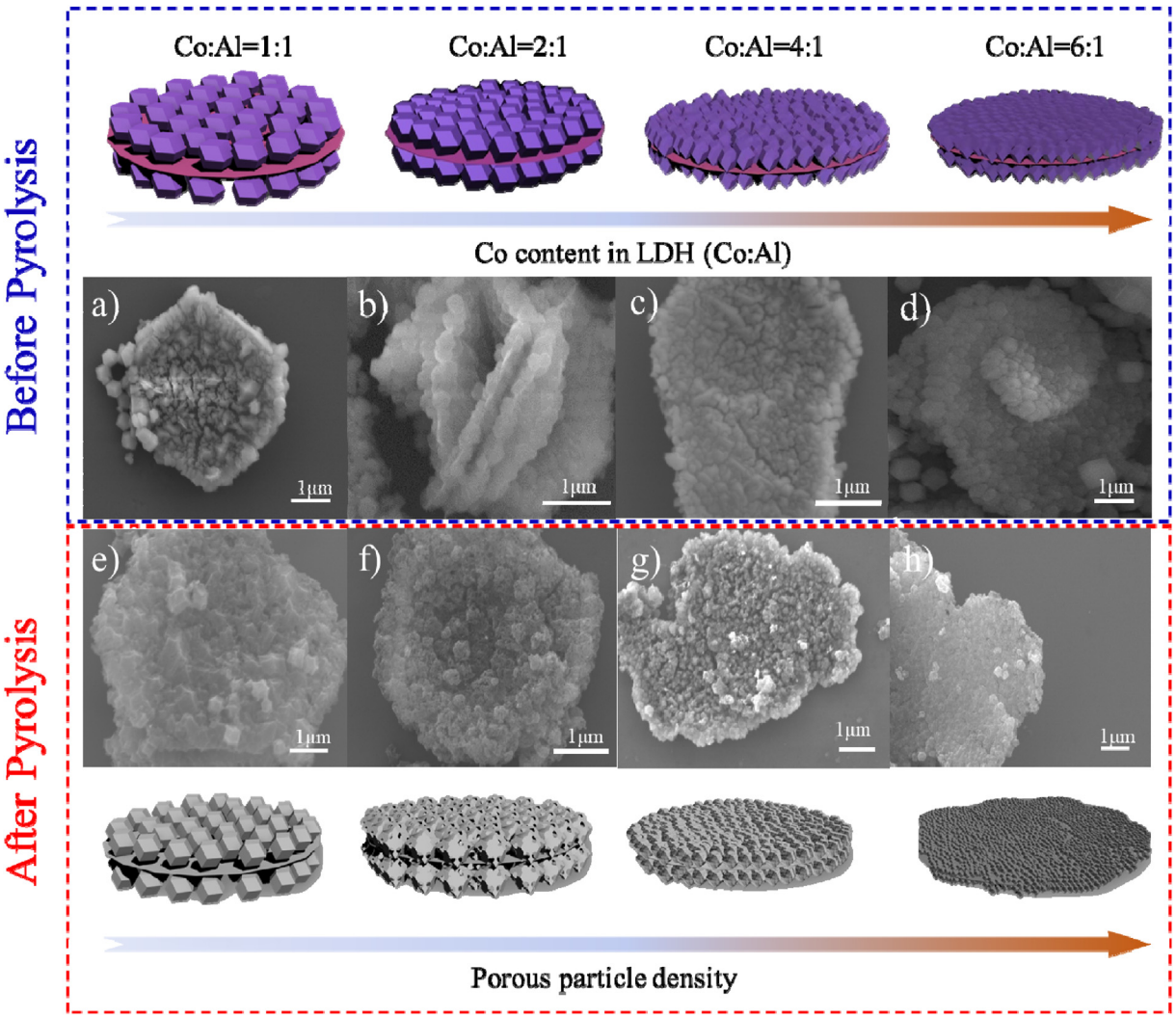

Fig. 2. SEM images of Pt@SLs-ZIF-67-LDH-x with different Co: AI molar ratios of a) 1:1, b) 2:1, c) 4:1, d) 6:1; SEM images of Pt3Co@SLs-MCPTx with different Co: AI molar ratios of e) 1:1, f) 2:1, g) 4:1, h) 6:1.

(Figure S4a). The pore analysis was carried out for these catalysts. As shown in Figure S4b, all the catalysts showed similar micropores centered at 3.7 nm, which indicated that the micropore was determined by ZIF crystal structure rather than the crystal density on the LDH surface. However, the mesoporous volumes of these catalysts showed a volcano-relationship with the content of Co in LDH, that was, it increased at a relatively low Co/Al ratio, and then decreased at high with Co content. These results meant that the meso-scale property could be modulated by Co content without changing other features, such as micropores, framework structures.

Figures S5a and S5b show that the largest double capacitance and highest electrochemical surface area (ECSA) were obtained on the Pt_3Co@SLs-MCPT2 catalyst modified electrode among the as-produced catalysts. The values of double capacitance and ECSA of these catalysts exhibited a similar trend to BET surface area as a function of Co content. This meant that the surface density of carbon framework did affect the electrochemical properties. The electrocatalytic activities of the catalysts for ORR tests were examined in 0.1 $mol \cdot L^{-1}$ $HClO_4$ using the typical three-electrode setup. The Pt_3Co@SLs-MCPT2 catalyst modified electrode showed the most positive half-wave potential ($E_{1/2}$, 0.92 V vs reference hydrogen electrode, RHE) among the produced catalysts, which was higher than that of commercial Pt/C by 40 mV. The specific activity (SA) and mass activity (MA) of these catalysts reached the highest values for Pt_3Co@SLs-MCPT2 (SA: 0.52 $mA \cdot cm^{-2}$; MA: 402 $mA \cdot mg_{Pt}^{-1}$) with the Co/Al ratio of 2. Further increased or decreased Co/Al ratio led to the decreased ORR activity (Fig. 3a and Figure S6), which was similar to the trend of ECSA and BET surface area values of

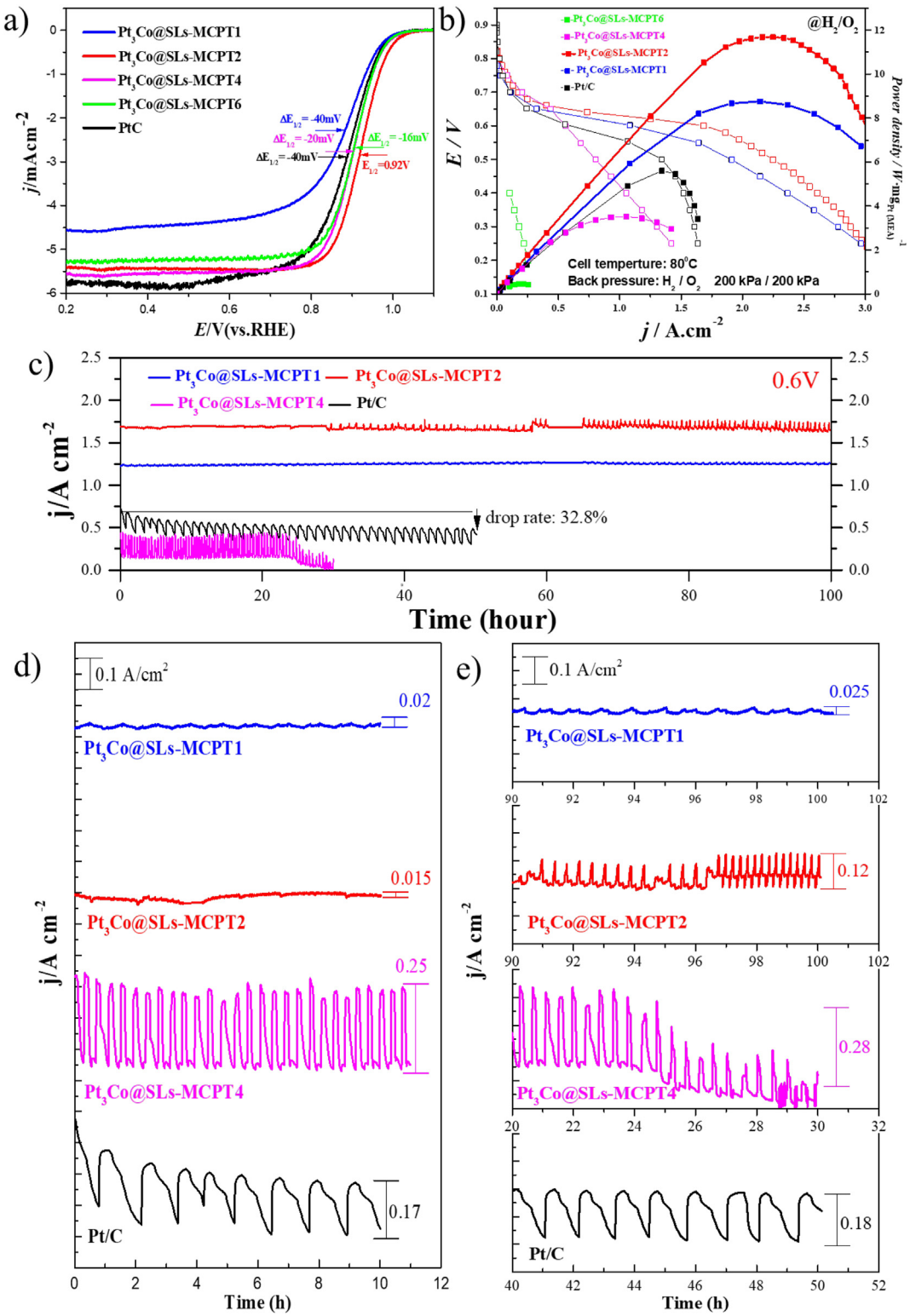

Fig. 3. (a) ORR polarization curves of Pt_3Co@SLs-MCPTx and commercial Pt/C recorded in O_2-saturated 0.1 mol·L^{-1} $HClO_4$ solution at room temperature; after iR-compensation (b) the voltages and power densities of the H_2/O_2 fuel cell employing Pt_3Co@SLs-MCPTx and commercial Pt/C, as the cathode; PtRu/C was used as the anode; the membrane used was Nafion-HP; data obtained at 80 °C. (c) Comparison of the fuel cell lifetime at 0.60 V over 100 h for the MEAs employing Pt_3Co@SLs-MCPTx and commercial Pt/C as the cathode, respectively, (d) comparison of the fuel cell lifetime at 0.60 V over first 10 h and (e) comparison of the fuel cell lifetime at 0.60 V over final 10 h are enlarged based on Fig. 3c.

these catalysts. These results indicated that the exposure of active sites and ORR activity are strongly related to the meso-scale property, i.e., the surface density of carbon frameworks.

We also analyzed the ORR activities of mesoporous carbon derived from the ZIF-67 alone (MCP), superlattice-like carbon frameworks without Pt NPs (SLs-MCPT) and PtCo alloy catalyst without superlattice structure (Pt_3Co@MCP) for comparison. As shown in Figure S7, none of them showed comparable activity to Pt_3Co@SLs-MCPT2 in terms of half-wave potential, indicating the excellent ORR activity originated from both unique superlattice-like meso-structure and Pt-rich hollow alloy nano-structure.

Furthermore, the performances of these produced catalysts in PEMFC were evaluated as the function of carbon framework density. The MEAs with 5 cm^2 active areas were fabricated by using Pt_3Co@SLs-MCPTX or commercial Pt/C as the cathode catalyst and commercial PtRu/C as the anode at a low Pt loading of 60 $\mu g \cdot cm^{-2}$ (each side). The exact Pt loading was measured after the test by inductively coupled plasma-atomic emission spectroscopy (ICP-AES) (Table S1). As shown in Fig. 3b, the peak power density and Pt utilization of cathodes fabricated by Pt_3Co@SLs-MCPTx catalysts increased when the Co/Al ratio increased from 1 to 2, and then decreased dramatically with a further increase of Co content. The highest specific power density (11.69 $W \cdot mg_{Pt}^{-1}$ (MEA)) had been obtained in a PEMFC catalyzed by Pt_3Co@C-SLS-2, which was 2.09 times of that by commercial Pt/C, ranked among the best catalysts published so far [26−29]. Notably, the Pt_3Co@SLs-MCPT4 and Pt_3Co@SLs-MCPT6 catalysts, which showed higher activity than those of Pt_3Co@SLs-MCPT1 and Pt/C catalysts in the RDE test, exhibited much worse performance in fuel cell. This result indicated that the meso-scale structure had a dominated impaction in the real fuel cell environment. The higher surface density of carbon frameworks would hinder the penetration of ionomer to form proton conductive network, leading to a low Pt utilization in fuel cell [26−28].

Then in order to evaluate the quality of power output, we analyzed the mass transfer capability of the prepared catalysts by using chronoamperometry. As the performance was dominated largely by mass transfer at a voltage around 0.6 V, we conducted the chronoamperometric tests under the voltage of 0.6 V [26,29,30]. As shown in Fig. 3c, no obvious decay of power output was observed during 100 h test for Pt_3Co@C-SLS-1 (0.75 $W \cdot cm^{-2}$) and Pt_3Co@C-SLS-2 (1.01 $W \cdot cm^{-2}$) fabricated MEAs, and the TEM image of Pt_3Co@C-SLS-2 after the stability test showed the average size of nanoparticles increased from 3.33 nm to 3.63 nm (Figure S8), demonstrating remarkable mass transfer capability, durability of the porous carbon framework catalysts, and restrained ability of the size growth. By contrast, a cell catalyzed by conventional Pt/C catalysts with the same Pt loading showed a power of 0.30 $W \cdot cm^{-2}$ with 32% current decay after 50 h test.

More importantly, the current density values of Pt_3Co@C-SLS-1 and Pt_3Co@C-SLS-2 catalyzed MEAs maintained at a relatively stable state with a fluctuation amplitude less than 25 $mA \cdot cm^{-2}$ at the beginning of operation (Fig. 3d). In sharp contrast, the MEAs fabricated by commercial Pt/C and Pt_3Co@C-SLS-4 catalysts outputted current unsteadily. Serious water flooding occurred at the beginning of operation in these two MEAs according to the high fluctuation amplitude. The fluctuation amplitudes of MEAs catalyzed by Pt_3Co@C-SLS-4 (250 $mA \cdot cm^{-2}$) and Pt/C catalysts (170 $mA \cdot cm^{-2}$) were one order higher than those of Pt_3Co@C-SLS-1 and Pt_3Co@C-SLS-2 catalyzed MEAs. These results signified that the meso-scale property of catalyst dominated the quality of power output in our case. In addition, the fluctuation amplitude seemed to be positively correlated with the surface density of carbon frameworks. As shown in Fig. 3e, the fluctuation amplitude increased with the increased of Co content. Specifically, the MEA fabricated by using Pt_3Co@C-SLS-1 catalyst could retain stable current output in 100 h with a small amplitude of 25 $mA \cdot cm^{-2}$. As for the Pt_3Co@C-SLS-2 catalyzed MEA, however, a sudden increase of fluctuation amplitude occurred after 30 h operation. When the Co/AI ratio increased to 4, the MEA fabricated by Pt_3Co@C-SLS-4 suffered from flooding with an amplitude of 280 $mA \cdot cm^{-2}$, which was similar to that of MEAs catalyzed by commercial Pt/C catalysts (180 $mA \cdot cm^{-2}$). Considering together with their similar micropores but different meso-scale structures, we could conclude that the meso-scale property had a high impact on the performance and lifetime of fuel cells. Just as shown in Fig. 4, the surface density of carbon frameworks, and the meso-scale property largely determined the channels for gas transfer and dewatering. The lower density meant larger channels and efficient mass transfer. After hours of operation, such carbon-based channels would be filled with some water, leading to the different abilities for continuous dewatering. The superlattice-like structure catalysts with adjustable density crystals showed powerful modulation on mass transport and antiflooding capability, then on the quality of fuel cell output.

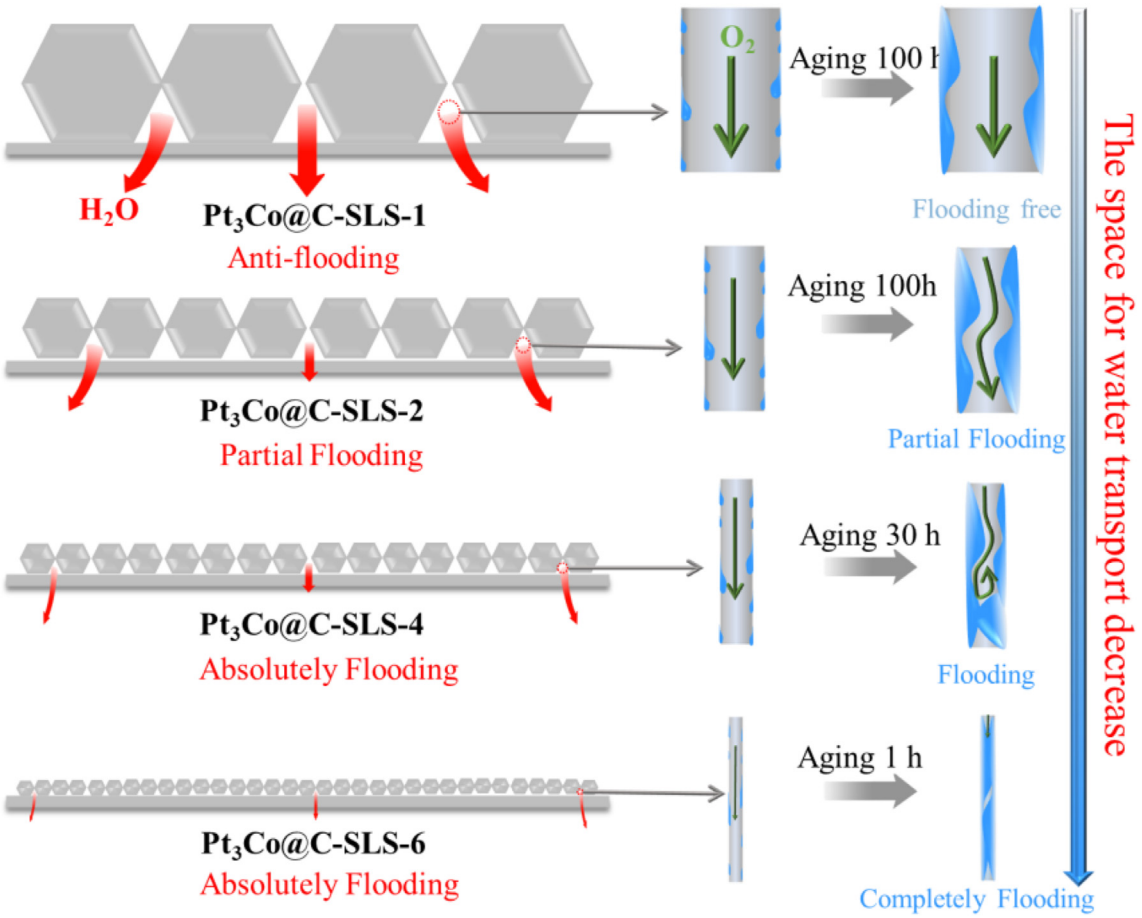

Fig. 4. Schematic illustration of the fuel cell operation of cathodes fabricated by Pt_3Co@SLs-MCPTx catalysts.

3. Conclusions

In summary, we reported a template-assisted epitaxial assembly way to fabricate bridged carbon nanotubes confined Pt_3Co alloy catalysts with superlattices-like structure. The favorable superlattices-like structure modulated by the Co content could lead to different mass transports and anti-flooding capabilities, which largely determined the quality of fuel cell during the continuous operation. Benefiting from the efficient mass transport capability of superlattices-like structure and highly efficient linkages of various species-transport channels, the higher quality power output with a current fluctuation less than 25 $mA \cdot cm^{-2}$ was achieved over 100 h. Also, the superlattices-like catalyst showed a high Pt utilization of 11.69 $W \cdot mg_{Pt}^{-1}$ (MEA) and durability in fuel cell.

Acknowledgements

This work was financially supported by the National Key Research and Development Program of China (2020YFB1506001), the National Natural Science Foundation of China (Grant Nos. 51772037, 52021004, 22022502, 21761162015, 22179012, 22208034, and the Program for the Top Young Innovative Talents of Chongqing (02200011130003), ang the graduate scientific research and innovation foundation of Chongqing (CYB20044).

References

[1] Wang G J, Yu Y, Liu H, Gong C L, Wen S, Wang X H, Tu Z K. Progress on design and development of polymer electrolyte membrane fuel cell systems for vehicle applications: a review[J]. Fuel Process. Technol., 2018, 179: 203−228.
[2] Kongkanand A, Mathias M F. The priority and challenge of high-power performance of low-platinum proton-exchange membrane fuel cells[J]. J. Phys. Chem. Lett., 2016, 7(7): 1127−1137.
[3] Ahluwalia R K, Wang X, Steinbach A J. Performance of advanced automotive fuel cell systems with heat rejection constraint[J]. J. Power Sources, 2016, 309: 178−191.
[4] Béthoux O, Cathelin J. Design of a high voltage input - output ratio dc-dc converter dedicated to small power fuel cell systems[J]. Eur. Phys. J.-Appl. Phys., 2010, 52(3): 31102.
[5] Sakka M A, Mierlo J V, Gualous H. Dc/Dc converters for electric vehicles[M]. Turkey: Seref S, 2011, 100: 466.
[6] Kolli A, Gaillard A, De Bernardinis A, Bethoux O, Hissel D, Khatir Z. A review on DC/DC converter architectures for power fuel cell applications[J]. Energy Convers. Manag., 2015, 105: 716−730.

[7] Wen H Q, Su B. Hybrid-mode interleaved boost converter design for fuel cell electric vehicles[J]. Energy Convers. Manag., 2016, 122: 477−487.
[8] Xu H P, Kong L, Wen X H. Fuel cell power system and high power DC-DC converter[J]. IEEE Trans. Power Electron., 2004, 19(5): 1250−1255.
[9] Tanrioven M, Alam M S. Modeling, control, and power quality evaluation of a PEM fuel cell-based power supply system for residential use[J]. IEEE Trans. Power Electron., 2006, 42(6): 1582−1589.
[10] Zenith F, Skogestad S. Control of fuel cell power output[J]. J. Process Control, 2007, 17(4): 333−347.
[11] Shen J, Xu L, Chang H W, Tu Z K, Chan S H. Partial flooding and its effect on the performance of a proton exchange membrane fuel cell[J]. Energy Convers. Manag., 2020, 207: 112537.
[12] Xing L, Shi W D, Su H N, Xu Q, Das P K, Mao B D, Scott K. Membrane electrode assemblies for PEM fuel cells: a review of functional graded design and optimization[J]. Energy, 2019, 177: 445−464.
[13] Laribi S, Mammar K, Sahli Y, Koussa K. Analysis and diagnosis of PEM fuel cell failure modes (flooding & drying) across the physical parameters of electrochemical impedance model: using neural networks method[J]. Sustain. Energy Technol. Assessments, 2019, 34: 35−42.
[14] Ijaodola O S, El-Hassan Z, Ogungbemi E, Khatib F N, Wilberforce T, Thompson J, Olabi A G. Energy efficiency improvements by investigating the water flooding management on proton exchange membrane fuel cell (PEMFC) [J]. Energy, 2019, 179: 246−267.
[15] Li Y H, Pei P C, Wu Z Y, Ren P, Jia X N, Chen D F, Huang S W. Approaches to avoid flooding in association with pressure drop in proton exchange membrane fuel cells[J]. Appl. Energy, 2018, 224: 42−51.
[16] Sun R L, Xia Z X, Shang L, Fu X D, Li H Q, Wang S L, Sun G Q. Hierarchically ordered arrays with platinum coated PANI nanowires for highly efficient fuel cell electrodes[J]. J. Mater. Chem., 2017, 5(29): 15260−15265.
[17] Zeng Y C, Shao Z G, Zhang H J, Wang Z Q, Hong S J, Yu H M, Yi B L. Nanostructured ultrathin catalyst layer based on open-walled PtCo bimetallic nanotube arrays for proton exchange membrane fuel cells[J]. Nano Energy, 2017, 34: 344−355.
[18] Tian Z Q, Lim S H, Poh C K, Tang Z, Xia Z T, Luo Z Q, Shen P K, Chua D, Feng Y P, Shen Z X, Lin J Y. A highly order-structured membrane electrode assembly with vertically aligned carbon nanotubes for ultra-low Pt loading PEM fuel cells[J]. Adv. Energy Mater., 2011, 1(6): 1205−1214.
[19] Steinbach A J, Debe M K, Pejsa M J, Peppin D M, Haug A T, Kurkowski M J, Hendricks S M. Influence of anode GDL on PEMFC ultra-thin electrode water management at low temperatures[M]. ECS Trans., 2011, 41: 449−457.
[20] Jiang S F, Yi B L. The progress of order-structured membrane electrode assembly[J]. J. Electrochem., 2016, 22(3): 213−218.
[21] Yan C, Wang T. A new view for nanoparticle assemblies: from crystalline to binary cooperative complementarity[J]. Chem. Soc. Rev., 2017, 46(5): 1483−1509.
[22] Li T T, Xue B, Wang B W, Guo G N, Han D D, Yan Y C, Dong A G. Tubular monolayer superlattices of hollow Mn_3O_4 nanocrystals and their oxygen reduction activity[J]. J. Am. Chem. Soc., 2017, 139(35): 12133−12136.
[23] Cheng K Y, Lin C H, Tzeng M C, Mahmood A, Saeed M, Chen C H, Ong C W, Lee S L. Superstructure manipulation and electronic measurement of monolayers comprising discotic liquid crystals with intrinsic dipole moment using STM/STS[J]. Chem. Commun., 2018, 54(58): 8048−8051.
[24] Ding J, Liu Z, Liu X R, Liu J, Deng Y D, Han X P, Zhong C, Hu W B. Mesoporous decoration of freestanding palladium nanotube arrays boosts the electrocatalysis capabilities toward formic acid and formate oxidation[J]. Adv. Energy Mater., 2019, 9(25): 1900955.
[25] Burian M, Karner C, Yarema M, Heiss W, Amenitsch H, Dellago C, Lechner R T. A shape-induced orientation phase within 3D nanocrystal solids[J]. Adv. Mater., 2018, 30(32): 1802078.
[26] Wang J, Wu G P, Wang W L, Xuan W H, Jiang J X, Wang J C, Li L, Lin W F, Ding W, Wei Z D. A neural-network-like catalyst structure for the oxygen reduction reaction: carbon nanotube bridged hollow PtCo alloy nanoparticles in a MOF-like matrix for energy technologies [J]. J. Mater. Chem., 2019, 7(34): 19786−19792.
[27] Wang J, Ding W, Wei Z D. Review: performance of polymer electrolyte membrane fuel cells at ultra-low platinum loadings[J]. Acta Phys. Chim. Sin., 2020, 37(9): 2009094.
[28] Wang J, Wu G P, Xuan W H, Peng L S, Feng Y, Ding W, Li L, Liao Q, Wei Z D. A framework ensemble facilitates high Pt utilization in a low Pt loading fuel cell[J]. Catal. Sci. Technol., 2021, 11(8): 2957−2963.
[29] Wang Y C, Lai Y J, Song L, Zhou Z Y, Liu J G, Wang Q, Yang X D, Chen C, Shi W, Zheng Y P, Rauf M, Sun S G. S-doping of an Fe/N/C ORR catalyst for polymer electrolyte membrane fuel cells with high power density[J]. Angew. Chem., Int. Ed., 2015, 54(34): 9907−9910.
[30] Wang M J, Zhao T, Luo W, Mao Z X, Chen S G, Ding W, Deng Y H, Li W, Li J, Wei Z D. Quantified mass transfer and superior antiflooding performance of ordered macro-mesoporous electrocatalysts[J]. AIChE J., 2018, 64(7): 2881−2889.

类超晶格结构：有序性传质赋予燃料电池高品质输出性能

王　健[a,#]，轩文辉[a,#]，何　倩[a]，蒋金霞[a]，周圆圆[a]，聂　瑶[b]，廖　强[c]，邵敏华[d]，丁　炜[a,*]，魏子栋[a,*]

[a] 重庆大学化学化工学院，洁净能源与资源化工过程重庆市重点实验室，重庆 401331，中国

[b] 重庆师范大学化学学院，绿色合成与应用重庆市重点实验室，重庆 401331，中国

[c] 重庆大学能源与动力工程学院，工程热物理研究所，重庆 400044，中国

[d] 化学与生物分子工程学院，香港科技大学，香港 999077，中国

摘要

质子交换膜燃料电池（PEMFC）是一种强耦合、复杂非线性、动态的、多输入多输出的能量转换装置，不容易达到或保持理想的工作状态。在动态的 PEMFC 的工作状态下，其输出的电流和电压是振动的、不稳定的，会对负载的使用和寿命造成很大的影响，严重时亦可损坏负载。该波动的电流或电压输出不仅直接决定着发电系统的成本，而且影响着有效的能量转换效率及电子原件和设备的寿命。基于此，本工作针对燃料电池动态特性及动态排水空间受限导致其电流不规则波动，进而影响输出电能品质和燃料电池系统及其他电子元件的寿命和维护成本等问题，开发了一种外延生长的方法制备排水空间可调控的抗溺水电极，通过调控载体的成核位点密度，形成一种具有不同排水空间的类超晶体结构微米级铂基催化剂。该催化剂制备的电极不仅表现出极佳的抗溺水性，在极低的电流振幅（25 $mA \cdot cm^{-2}$）下持续稳定的输出高品质电能，同时提高了铂的利用率，使其组成的 MEA 比功率密度达到 11.69 $W \cdot mg_{Pt}^{-1}$，表现出极高的应用潜力。

关键词：传质；PtCo 合金；电能品质；类超晶格；氧还原